CdS−ZnS Core−Shell Nanoparticle Formation: Experiment, Mechanism, and Simulation

Mani Ethayaraja, Chettiannan Ravikumar, Devarajan Muthukumaran, Kanchan Dutta, and Rajdip Bandyopadhyaya*

Department of Chemical Engineering, Indian Institute of Technology Kanpur, Kanpur 208016, India

Received: September 17, 2006; In Final Form: December 22, 2006

CdS−ZnS core−shell nanoparticles are synthesized in a series of water-in-oil microemulsion solutions with increasing microemulsion drop sizes. Shell formation was confirmed by observation of a red shift in the UV−vis absorption spectra. Nanoparticle diameter and shell thickness estimated independently from the spectra and from mass balance approximation are consistent with each other. A new two-stage mechanism of core−shell nanoparticle formation has been developed from the experimental findings that consists of coalescence-exchange of microemulsion drops with nucleation, growth, and coagulation of particles. Quantitative predictions from Monte Carlo simulation of this mechanism compares well with the temporal evolution of experimental mean nanoparticle diameter and shell thickness for most of the cases, except when the nature of water in the microemulsion drops is different from bulk water for very small drop size. An increase in both the core and core−shell nanoparticle diameter with drop size reflects the control of the microemulsion template structure on nanoparticle synthesis.

1. Introduction

Semiconductor nanoparticles have attracted great interest in both theoretical research and technological applications.[1] Size dependence of band gap in these nanoparticles due to quantum confinement effect[2] has been utilized to control the photoluminescence (PL) color from blue to red by preparing nanoparticles of different size.[3] The control of luminescence color and its purity can be achieved by manipulating the size and shape of the nanoparticles. However, the brightness of luminescence or quantum yield (QY) and photostability of nanoparticles are poor due to the presence of surface traps.[3] The maximum QY reported was in the range of 10−25%.[4] Subsequently, it was shown that inorganically or organically passivated (e.g., by amines) nanoparticles can have enhanced QY up to 50%.[4] Mekis et al.[5] demonstrated that QY can be increased up to a maximum of 85% at room temperature by forming a shell of higher band gap CdS around CdSe nanoparticles (CdSe−CdS). Enhancement of QY was attributed to effective passivation of surface traps by formation of the shell, whose thickness is an important parameter to manipulate optical properties.[6,7] Other than enhancement of optical properties, core−shell nanoparticles show very high reactivity in photochemical reactions compared to core nanoparticles.[8,9] Several different combinations of core−shell nanoparticles, such as CdSe−ZnS,[4,7] CdS−ZnS,[8−11] CdSe−CdS,[5,6] CdS−PbS,[12] CdS−HgS,[13] and CdS−Ag_2S,[14,15] have been synthesized and studied for their photoluminescence properties.

The most common solution-based methods for nanoparticle synthesis with precise control of size and shape are organometallic[16] and water-in-oil (w/o) microemulsion routes.[17] In the former, organic metal precursors are heated to high temperatures (250−300 °C) in a coordinating solvent, leading to a reaction of precursors, nucleation, and growth of nanoparticles. This method has been extensively used for the synthesis of II−VI and III−V semiconductors[18] and metals also. Size-control is achieved by varying reaction temperature, initial precursor concentration, and by further intermediate injection of precursors, if necessary. In contrast, w/o microemulsions are self-assembled surfactant templates of nanometer size, which can be spherical, cylindrical, or of other desired shape, dispersed in a continuous oil medium. Water with a predissolved reactant added into the microemulsion solution goes only inside the templates and thereby forms nanometer-sized spherical water drops, acting as size and shape controlled nanoreactors.[17] Appropriate reactants in the water drops of two different microemulsions are mixed together for nanoparticle synthesis by reactive precipitation. The drops collide because of Brownian motion, occasionally coalesce, and exchange their contents thus bringing the two reactants together inside a single drop for reaction. If insoluble in water, the reaction product nucleates to form a solid nucleus within the drop. The nucleus grows further by deposition of additional dissolved product molecules, mediated by coalescence and exchange with other drops.

The microemulsion route is therefore a more general strategy: one can utilize the control in size and shape of its drops and take advantage of the confinement of reactants and products within the drop for nanoparticle synthesis, in contrast to the bulk-solution based organometallic route. Thus, w/o microemulsions have been used for the synthesis of an extensive range of nanomaterials: metals,[19] semiconductors,[20] metal carbonates,[21] hydroxides, and even water soluble compounds[22] and organics,[23] the last two of which were obtained by small modifications in the above scheme. Further attractiveness of the microemulsion route is attributed to the ability of manipulating spatial confinement of reactants in the nanoscale and control over their coalescence-exchange dynamics. Confinement can be altered on changing the diameter of spherical water drops from 2 to 18 nm, which is done by increasing water to surfactant molar ratio (R).[24] Similarly, coalescence-exchange rate of water drops can be varied over 2 orders of magnitude by changing the oil phase, nature of surfactant, or temperature.[25] For example,

* To whom correspondence should be addressed. E-mail: rajdip@iitk.ac.in. Phone: 91-512-259 7697. Fax: 91-512-259 0104.

10.1021/jp066066j CCC: $37.00
Published on Web 02/03/2007

the rate of a chemical reaction can be reduced by orders of magnitude if it is conducted in a w/o microemulsion rather than in a bulk aqueous medium. This is because the reactants are partitioned in different water drops, and the time scale of coalescence-exchange of these drops are few orders less than the diffusion time scale of the reactant in bulk. Therefore, these possibilities offer additional control parameters other than concentration of reactants and surfactants for the synthesis of size- and shape-controlled nanostructures.

The present work focuses on developing a mechanism for core−shell nanoparticle formation based on our experiments in CdS−ZnS system. On the basis of this mechanism, we use Monte Carlo (MC) simulation for quantitative prediction of nanoparticle diameter and shell thickness. This will elucidate the role of spatial confinement at nanoscale, Brownian collision of drops, and molecular exchange and partitioning of various reactants between drops on the process of nanoparticle synthesis; thus setting it apart from other bulk-phase crystallization or precipitation studies.

2. Experimental

2.1. Synthesis of CdS Core and CdS−ZnS Core−Shell Nanoparticles. AOT [Sodium bis(2-ethylhexyl)sulfosuccinate] surfactant (99% pure) and isooctane (2,2,4-trimethyl pentane) (99% pure) were purchased from Sigma and Qualigen, respectively. Cadmium nitrate (99% pure), zinc nitrate (99% pure), and sodium sulfide (55% pure) were purchased from Merck. All chemicals were used as received. Deionized Millipore-Milli-Q water was used in all the experiments. A stock solution of 0.1 M AOT in isooctane was utilized throughout.

In a typical experiment, a w/o microemulsion solution containing $Cd(NO_3)_2$ (solution A) was prepared by mixing the appropriate volumes of aqueous $Cd(NO_3)_2$ solution with the AOT stock solution so as to yield microemulsions with different R values, ranging from 2 to 15. An overall concentration of $Cd(NO_3)_2$ equal to 0.0018 M with respect to the total microemulsion volume (oil and water) was maintained for each R so that the total amount of CdS available for nanoparticle formation was constant in all experiments. Similarly, another w/o microemulsion containing Na_2S (solution B) was prepared with overall Na_2S concentration twice that of $Cd(NO_3)_2$ (i.e., 0.0036 M). Microemulsion C, similar to A in other respects but having $Zn(NO_3)_2$ instead of $Cd(NO_3)_2$, was also made. A fourth microemulsion solution was made without any dissolved salt and is only to be used as a reference in UV−vis absorption spectra measurements. All the microemulsions (A, B, C, and reference) were sonicated for 20 min to keep them stable throughout the process of synthesis and characterization. We verified that sonication did not affect the diameter of nanoparticles synthesized by us. However, if the reactant concentration and R is increased, higher sonication time may be required. CdS nanoparticles were prepared in a quartz cuvette by rapid transfer and instantaneous mixing of 1 mL of each of microemulsion A and B solutions. UV−vis absorption spectra of CdS nanoparticles were recorded in situ using Elico SL159 UV−vis spectrophotometer. After 200 s, 1 mL of microemulsion C was added to the cuvette and was mixed instantaneously. During this second stage of synthesis, excess Na_2S reacts with $Zn(NO_3)_2$ to form ZnS, which grows as a shell on the preformed CdS nanoparticles. This was also observed by recording the absorbance spectra as a function of time. An experiment with increasing R amounts to nanoparticle formation with increased drop size. All the experiments were conducted at a room temperature of 28 °C.

2.2. Calculation of Core and Core−Shell Nanoparticle Diameter. The recorded absorption spectra of nanoparticles (CdS and CdS−ZnS) were used to determine their diameter. The band gap of CdS nanoparticles is obtained by using the equation[26]

$$(\sigma h\nu)^2 = k(h\nu - E_g) \tag{1}$$

In eq 1, σ is molar absorption coefficient of nanoparticles, which is obtained from the measured absorption spectra using Beer−Lambert's law, $h\nu$ is photon energy, k is a proportional factor, and E_g is band gap of nanoparticles with the latter being a function of diameter. A plot of $(\sigma h\nu)^2$ versus $h\nu$ shows an intermediate linear region (as given by eq 1), from which one calculates E_g by data fitting. The diameter of core CdS nanoparticle is then calculated from the following equation[27]

$$E_g = E_{gb} + \frac{h^2}{2d_p^2}\left(\frac{1}{m_e} + \frac{1}{m_h}\right) - \frac{3.6e^2}{4\pi\epsilon d_p} \tag{2}$$

where E_{gb} is bulk band gap (2.5 eV for CdS and 3.7 eV for ZnS), h is Planck's constant, d_p is diameter of nanoparticle, m_e (0.19 m_0 for CdS and 0.25 m_0 for ZnS, where m_0 is the free electron mass) and m_h (0.8 m_0 for CdS and 0.59 m_0 for ZnS) are the effective electron and hole masses, respectively, e is the electronic charge, and ϵ is the dielectric constant of nanoparticle (5.7 ϵ_0 for CdS and 5.2 ϵ_0 for ZnS, where ϵ_0 is the dielectric constant of vacuum).[9]

A direct method for the estimation of outer diameter of CdS−ZnS core−shell nanoparticle and hence ZnS shell thickness (from UV−vis absorption spectra of core−shell nanoparticles) is not available to the best of our knowledge. Therefore, we calculate the outer diameter of core−shell nanoparticle from its spectrum, assuming as if the whole nanoparticle consists of only CdS. This will be a reasonable assumption in view of the small shell thickness, compared to the core nanoparticle diameter.

In another alternative approach, we have calculated the thickness of the ZnS shell by using a simple mass balance based on amount of ZnS that can form. For a spherical nanoparticle of core diameter d_p and shell thickness δ, the shell volume, V_s, is given by

$$V_s = \frac{\pi}{6}[(d_p + 2\delta)^3 - d_p^3] \tag{3}$$

Assuming all the shell material (ZnS) is used for deposition and growth on the existing CdS core nanoparticles, we have

$$V_s = \frac{nM}{N_p\rho_s} = \frac{\pi}{6}[(d_p + 2\delta)^3 - d_p^3] \tag{4}$$

where n is the number of moles of ZnS that can form by reaction, M and ρ_s are molecular weight and density of ZnS, respectively, and N_p is the number of core nanoparticles. Using eq 4, shell thickness δ can be estimated. Prior to that, d_p is calculated using the UV−vis spectra of CdS core nanoparticles and N_p is estimated from the known concentration of CdS and d_p.

3. Results and Discussion

3.1. UV−vis Absorption Spectra of Nanoparticles. Figure 1a shows UV−vis absorption spectra of as-prepared CdS nanoparticles,on increasing R from 2 to 15. The spectra were taken at 90 s (approximately) after instantaneous mixing of

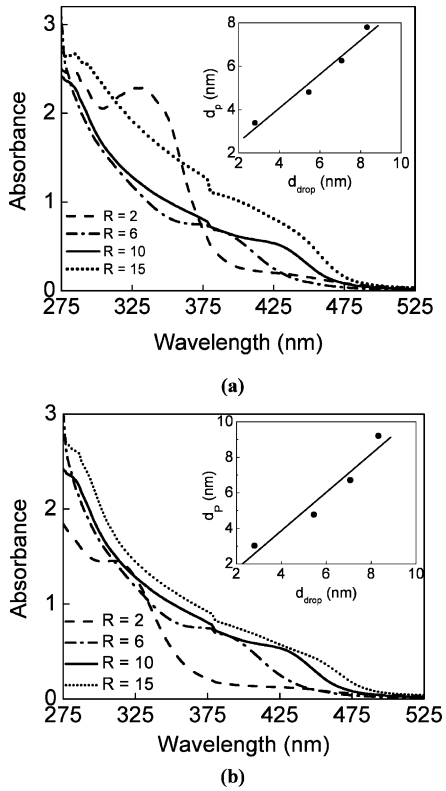

Figure 1. UV−vis absorption spectra of (a) core CdS nanoparticles at time $t = 90$ s, for $[Cd^{2+}] = 0.0018$ M and $[S^{2-}] = 0.0036$ M and [AOT] = 0.1 M. Inset shows measured mean CdS diameter vs drop size. (b) Final CdS−ZnS core−shell nanoparticles at time $t = 20$ min on addition of $[Zn^{2+}] = 0.0018$ M to the microemulsion solution in (a). Inset shows measured mean CdS−ZnS diameter vs drop size. Lines in both the insets are best linear fits to the measured particle diameter.

microemulsions A and B at room temperature. Since CdS nanoparticles have size dependent band gap, the peak position attributed to 1s-1s transition is dependent on particle size.[28] All the samples showed absorption peak at smaller wavelengths compared to bulk CdS, which shows a peak at 512 nm. This confirms the formation of CdS nanoparticles. As shown in Figure 1a, the peak position continuously shifts toward higher wavelength (red shift) as R increases, implying the diameter of the CdS core increases with R. For $R = 2$, the peak position is at 331 nm, which corresponds to a nanoparticle diameter of 3.4 nm, while for $R = 6$, the peak position is at 377 nm, which implies a particle diameter of 4.8 nm. For $R = 6$, Hirai et al.[20] reported 380 nm as the peak position, which is very close to ours. Another feature in the spectra of Figure 1a is the shape of the absorption curve. Nanoparticles synthesized at smaller R showed relatively sharper absorption peak compared to those prepared at higher R. This broadness in the absorption spectra may be because of increased polydispersity[18] at higher values of R. The inset in Figure 1a shows a linear increase in nanoparticle diameter with microemulsion drop size, demonstrating the expected control of template size in nanoparticle synthesis.

Figure 1b shows the corresponding UV−vis absorption spectra of the CdS−ZnS core−shell nanoparticles. The latter are formed upon instantaneous addition of microemulsion C to the respective core CdS nanoparticle suspensions (at about 200 s) depicted in Figure 1a. The spectra in Figure 1b do not show any characteristic peak for ZnS particles, which rules out the possibility of formation of either individual ZnS or composite $Cd_xZn_{1-x}S$ nanoparticles.[9] For all R, the peak positions of core−shell spectra are red-shifted compared to their corresponding core CdS nanoparticles. This clearly indicates an increase in the overall nanoparticle diameter, as a result of growth of the ZnS shell around the core particles. Similar observation of red shift during shell growth have been made in other core−shell systems (CdSe−CdS, CdSe−ZnS, etc.) also.[5,7] In addition, both CdS and ZnS crystallize in a hexagonal wurtzite structure, suggesting the possibility of epitaxial growth of ZnS on CdS in our experiments. Indeed, Youn et al.[8] had proposed epitaxial growth as a mechanistic model for the shell growth of ZnS on CdS nanoparticles. Finally, the inset in Figure 1b shows that the outer diameter of the CdS−ZnS core−shell nanoparticle also increases linearly with drop size, again affirming the role of template structure and dynamics.

3.2. Nanoparticle Formation Mechanism and MC Simulation. The primary advantage with our MC simulation technique is its ability to address dynamically evolving transport and reacting systems, consisting of different elementary random events as part of the overall synthesis process. In the nanoparticle formation, these random events are coalescence-exchange of water drops leading to exchange of drop contents (both reactants and products), nucleation to form a solid particle, and growth of nanoparticles due to coalescence-exchange with other drops. In addition to these processes, as the nanoparticles grow bigger, van der Waals attraction becomes stronger for equal sized nanoparticles,[29] leading to coagulation of particles during drop−drop collisions. However, the growth of nanoparticle via coagulation may be limited by the size of the drops because a substantial amount of energy would be required to increase the drop size, as the surfactant film covering the drop has a finite bending modulus. Finally, when the nanoparticle reaches a diameter close to that of the drop the particles are stabilized in solution because of van der Waals attraction between particles being counterbalanced by steric repulsion of AOT surfactant molecules. Jain et al.[30] found that MC simulation of core nanoparticle formation without coagulation resulted in significantly smaller diameter than experimental data in literature,[20] pointing to the need for nanoparticle coagulation.

On the basis of their experiments, Zhou et al.[12] proposed an ion displacement mechanism for the formation of CdS−PbS core−shell nanoparticles. They added Pb^{2+} ions to an aqueous dispersion of CdS nanoparticles, stabilized by polyvinyl pyrrolidone (PVP). The authors hypothesized that Pb^{2+} ions displace Cd^{2+} ions from the external surface of CdS nanoparticles, and may further diffuse inside the core CdS structure also, thus forming a shell of PbS inside the original CdS nanoparticle. While making CdS−Ag_2S core−shell nanoparticles, but in w/o microemulsions (with no excess S^{2-} ions), Han et al.[15] also supported the ion displacement mechanism. However, ion displacement is not a general mechanism for core−shell nanoparticle formation. In both the above cases, Pb^{2+} or Ag^+ can replace Cd^{2+}, as the latter has a higher Gibbs free energy of hydration.[31]

Recently, Jain et al.[32] did MC calculations for CdS−Ag_2S core−shell particle formation based on partial implementation of the ion displacement mechanism, to predict the data of Han et al.[15] In their simulation, Ag^+ ions displace the Cd^{2+} ions only from the external surface of CdS nanoparticles, restricting them to the formation of only one monolayer of Ag_2S, which is not supported by other experiments in which multiple layers of shell are formed.[5,6,12]

For our system of CdS−ZnS particles, ion displacement mechanism by proposition can result only from the replacement

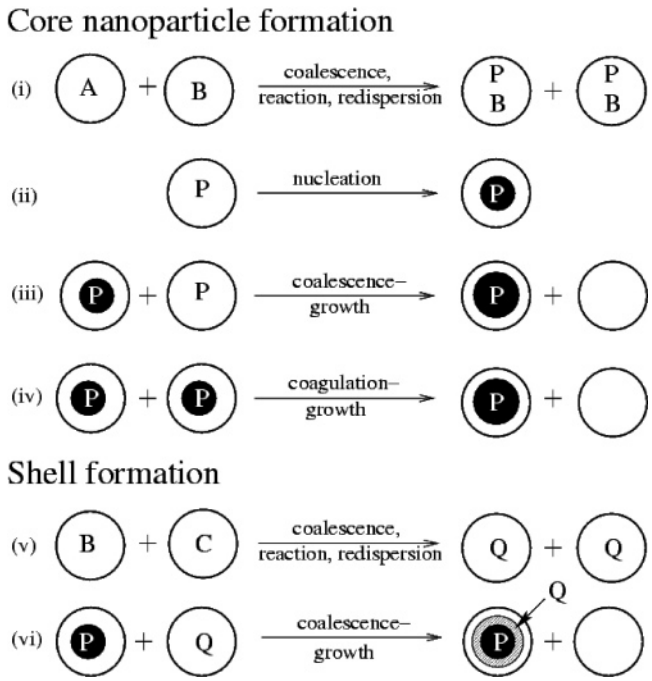

Figure 2. Various elementary steps involved in the formation of core (CdS) and core−shell (CdS−ZnS) nanoparticles on using excess of reactant B.

of Cd^{2+} ions from the outer layer of CdS nanoparticles by Zn^{2+} ions. This would have resulted in only the formation of a monolayer of ZnS over the preformed core CdS nanoparticle. Thus, it fails to explain a finite ZnS shell thickness of 0.35 to 0.8 nm (which consists of more than a layer of ZnS) observed in our own experiments or other similar literature reports.[5,6,12] Ion displacement therefore does not allow the core−shell particle to have a diameter greater than that of the core particle.

Second, the Gibbs free energy of hydration of Zn^{2+} ion is higher than that of Cd^{2+} ion.[31] Therefore, Zn^{2+} from the surrounding aqueous solution cannot displace Cd^{2+} of the CdS nanoparticle because such a replacement is not thermodynamically favorable. Hence, the observed formation of CdS−ZnS core−shell nanoparticle of a finite shell thickness cannot take place by ion-displacement.

Hence, we think that ZnS molecules form within water drops as a result of reaction between $Zn(NO_3)_2$ and excess Na_2S and then deposit and grow as a shell on the preformed core CdS nanoparticle. This mechanism is based on the series of UV−vis spectra recorded by us, confirming there is no separate core ZnS nanoparticle formation, rather the formation of a ZnS shell of finite thickness over the core CdS particle. This mechanism also successfully predicts most of our experimental observations and data on particle diameter.

Therefore, we propose an alternate and more general mechanism for core−shell nanoparticle formation, which explains the increase in overall core−shell nanoparticle diameter due to formation and deposition of shell material on the core nanoparticle. We validate our mechanism by comparing our own experiments and MC simulation to capture the dynamic evolution in both core and core−shell nanoparticle diameter.

Our mechanism consists of two stages: core nanoparticle formation[33−35] and shell growth. The core particle formation involves the following sequential steps [Figure 2 (i)−(iv)]

$$\text{(i) } A + B \xrightarrow{\text{reaction}} P(l_i)$$

$$\text{(ii) } P(l_i) \xrightarrow{\text{nucleation}} P(s_i)$$

$$\text{(iii) } P(l_i) + P(s_j) \xrightarrow{\text{coalescence-growth}} P(s_{i+j})$$

$$\text{(iv) } P(s_i) + P(s_j) \xrightarrow{\text{coagulation-growth}} P(s_{i+j})$$

The first sequence denotes the reaction step when two drops coalesce with reactants A and B, respectively, resulting in the formation of product $P(l_i)$, which is a drop with i number of liquid molecules of product P. This step is followed in the second sequence by nucleation of $P(l_i)$ to form $P(s_i)$, which is a drop with i number of solid molecules of product P, in the form of a nanoparticle. The third sequence represents growth of a nanoparticle present in one drop, $P(s_j)$, by the consumption of liquid product molecules, $P(l_i)$, of another drop during coalescence of these two drops. The last step describes coagulation of two nanoparticles belonging to two drops that in general can be of different diameters. Shell formation mechanism can be represented by the following sequence of events [Figure 2 (v)−(vi)]

$$\text{(v) } B + C \xrightarrow{\text{reaction}} Q(l_i)$$

$$\text{(vi) } P(s_j) + Q(l_i) \xrightarrow{\text{coalescence-growth}} Q(s_i) \text{ on } P(s_j)$$

The reaction between added reactant C with excess reactant of the first phase (B) produces the shell product $Q(l_i)$. The latter does not nucleate on its own in the presence of core nanoparticles, $P(s_j)$. Therefore, it deposits and grows on $P(s_j)$ forming a shell around the latter.

The core−shell nanoparticles do not coagulate unlike the core particles themselves. After the core formation stage (until 200 s), the diameter of a CdS nanoparticle was found to be ∼80% of the drop diameter for different values of R. Therefore, coagulation of two core−shell nanoparticles would have produced a particle of diameter larger than that of an individual drop, which would result in nanoparticles with incomplete coverage of adsorbed surfactants, a potentially unstable suspension. Thus, drop diameter is used as a constraint on the maximum nanoparticle diameter.

We implement the above mechanism in a MC simulation scheme. It begins with N number of drops (typically of the order of 10^5) with half of them containing reactant A and other half containing reactant B. In experiments, reactant B is taken twice in excess of reactant A, hence the mean number of reactant B molecules per drop is twice that of reactant A. At time $t = 0$, the number of individual reactant molecules (A and B) in each drop is taken to be independent Poisson distributions with the distribution means equal to the average number of respective A and B molecules per drop.[36] Simulation is based on interval of quiescence (IQ),[37] which is calculated from the total frequency of coalescence-exchange and nucleation, the two random events in nanoparticle synthesis

$$\tau = \frac{-\ln(1 - U)}{f_t} \tag{5}$$

where the total frequency $f_t = f_c + f_n$, and U is an uniformly distributed random number in [0, 1). Reaction of A and B to form P(l) and growth of P(s) by consuming P(l) in a drop are assumed instantaneous.[33] The frequency of coalescence-exchange (f_c) is calculated as

$$f_c = \frac{1}{2}\beta_d q_d N_{drop} N \tag{6}$$

where collision frequency (q_d) is obtained from the Smoluchowski equation[38]

$$q_d = \frac{8k_B T}{3\eta} \tag{7}$$

Here β_d is the coalescence efficiency and N_{drop} is the number density of drops, k_B is the Boltzmann constant, T is the temperature, and η is the viscosity of oil.

Total nucleation frequency is obtained by summing the individual frequencies in each drop as

$$f_n = \sum_{j=1}^{N} k_{n,j}(i) \tag{8}$$

where nucleation frequency in the jth drop, $k_{n,j}(i)$, is defined as[39]

$$\begin{aligned} k_{n,j}(i) &= 0 && \text{if } i < n^* \\ &= ik_0 \exp\left(\frac{-16\pi\gamma^3 v_m^2}{3(k_B T)^3(\ln[\lambda(i)])^2}\right) && \text{if } i \geq n^* \end{aligned} \tag{9}$$

In eq 9, k_0 is the pre-exponential term, n^* is the critical number of CdS molecules required for the formation of a stable nucleus, γ is the interfacial tension between CdS nanoparticle and water, v_m is the volume of one CdS molecule, and λ is the supersaturation of CdS.

Finally, event selection in MC simulation is based on probability of occurrence of ith event, which is

$$p_i(t) = \frac{f_i}{f_t(t)} \quad i = c \text{ or } n \tag{10}$$

If $0 \leq U < p_c$, any two drops are randomly selected for coalescence. If they have reactant A and B respectively, the product molecules P(l) form instantaneously. P(l) and excess reactant molecules (can be either A or B for a given drop-pair) are redistributed binomially over the two daughter drops. Binomial redistribution is well-established experimentally.[36] If however, one of the colliding drops has a particle, then all the P(l) molecules formed leads to growth of this particle and excess reactant is binomially redistributed. Finally, if both the drops have particles then the two particles coagulate to form a single particle and the latter grows by using all P(l) molecules available in these two drops. If the final particle diameter after coagulation is bigger than that of an individual drop, then coagulation is not physically possible. Drop diameter, therefore, acts as a constraint to particle diameter.

If $p_c \leq U < 1$, nucleation is due. Because of nonuniform distribution of P(l) in drops, nucleation rates of each drop can be different. Therefore, the ith drop can nucleate if it satisfies the following criterion

$$\left(p_c + \frac{\sum_{j=1}^{i-1} k_{n,j}(l,t)}{\sum_{j=1}^{N} k_{n,j}(l,t)}\right) \leq U < \left(p_c + \frac{\sum_{j=1}^{i} k_{n,j}(l,t)}{\sum_{j=1}^{N} k_{n,j}(l,t)}\right) \tag{11}$$

TABLE 1: Parameters Used in MC Simulation

variables	values	reference
d_{drop}[b] ($R = 2$)	2.8×10^{-9} m	[a]
d_{drop} ($R = 6$)	5.45×10^{-9} m	20
d_{drop} ($R = 10$)	7.07×10^{-9} m	20
d_{drop} ($R = 15$)	8.32×10^{-9} m	41
k_0	278.42 s^{-1}	33
K_s[c]	3.6×10^{-29} $mol^2 L^{-2}$	33
N	100 000	optimized
n^*	2	33
N_{drop}[d] ($R = 2$)	3.1190×10^{23} m^{-3}	calculated
N_{drop} ($R = 6$)	1.2624×10^{23} m^{-3}	calculated
N_{drop} ($R = 10$)	9.5552×10^{22} m^{-3}	calculated
N_{drop} ($R = 15$)	8.7182×10^{22} m^{-3}	calculated
T	301 K	measured
β_d ($R = 2$)	10^{-4}	typical value
β_d ($R = 6$)	10^{-4}	typical value
β_d ($R = 10$)	10^{-4}	typical value
β_d ($R = 15$)	10^{-4}	typical value
η	0.001 kg m^{-1} s^{-1}	standard value
γ	0.097 N m^{-1}	33

[a] d_{drop} for $R = 2$ is calculated by linear interpolation of data (d_{drop} for $R = 6$, 10, and 15) from refs 20 and 41. [b] d_{drop} = diameter of a water drop. [c] K_s = solubility product of CdS, used to calculate supersaturation in eq 9. [d] N_{drop} = total number density of water drops in a w/o microemulsion.

Simulation of this first stage of core formation is continued for 200 s, until microemulsion C is added.

Simulation of shell growth begins with only B molecules as excess reactant (all A is reacted by now) and some of these drops having P(s) particles. In addition, another $N/2$ number of drops with reactant C (distributed according to Poisson distribution) are also added to the N drops already present from first stage, thereby producing Q(l). Therefore this phase consists of only coalescence-exchange of drops with no new nucleation or particle coagulation. IQ is now calculated by replacing N with $3N/2$ in eqs 6, 8, and 11. Coalescence-exchange is done as before, except that coagulation of core−shell nanoparticles does not occur. Simulation is continued until all ZnS has grown as shell. The parameters and constants used in MC simulation are given in Table 1.

3.3. Comparison of Experiment and Simulation. Comparison of temporal evolution of nanoparticle diameter, both from experiments (UV−vis spectroscopy and mass balance method) and MC simulation, are shown in Figure 3. Filled symbols in Figure 3 show the diameter of the core CdS nanoparticle calculated using the measured UV−vis spectra (based on data from Figure 1 and eqs 1 and 2). Very good reproducibility of experimental data is seen, as evidenced by two separate experimental runs represented by triangular and circular symbols, respectively. A linear increase in core CdS diameter as a function of drop diameter (or R), as shown in inset of Figure 1, is evident from the data in Figure 3 also. In particular, the core CdS diameter increases from 3.4 to 7.8 nm, as R increases from 2 to 15.

Figure 3 also shows the final outer diameter of CdS−ZnS core−shell nanoparticle (open star symbols) from the mass balance method (eq 4). It increases from 4.1 to 9.4 nm, as R increases from 2 to 15, implying that ZnS shell thickness increases from 0.35 to 0.8 nm with R. Next, we compared these experimental values of core CdS diameter and the final CdS−ZnS core−shell diameter with predictions from our MC simulation scheme.

The simulation results (shown as a solid line in Figure 3) compare well with both core CdS (filled symbols) and the final CdS−ZnS core−shell nanoparticle diameter (open star symbols)

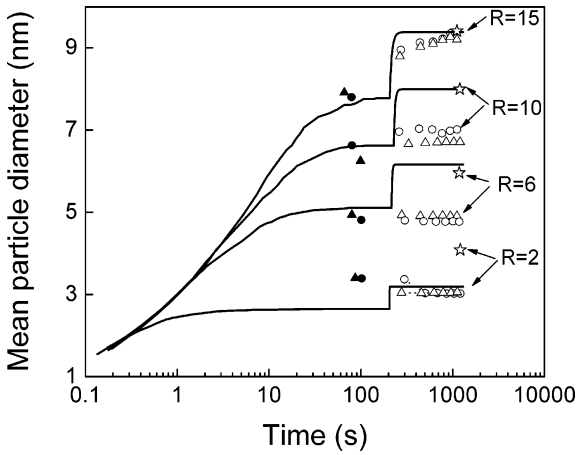

Figure 3. Comparison of temporal evolution of core CdS and core−shell CdS−ZnS nanoparticle diameter between MC simulation and experiments for various *R*. Concentrations used are $[Cd^{2+}] = 0.0018$ M, $[S^{2-}] = 0.0036$M, $[Zn^{2+}] = 0.0018$M, and [AOT] = 0.1 M. Data from sample repeated runs for each *R* also are shown, indicated by circular and triangular symbols, respectively. Description of symbols: (—), MC simulation; (●, ▲), core CdS nanoparticle diameter (calculated from UV−vis spectra); (○, Δ), outer diameter of CdS−ZnS core−shell nanoparticle (approximated from UV−vis spectra); (☆), final CdS−ZnS core−shell nanoparticle diameter (from mass balance method).

for all *R* values, except for $R = 2$. For $R = 2$, simulation underpredicts nanoparticle diameter compared to experiments. This is because of the different nature of water for very low values of *R*, since under these conditions the water present in the core of the microemulsion drop has a strong confined nature. It is influenced by the polarity of the ionic head groups of the surfactant molecules and is known to be different in property from bulk water.[40]

Simulation, in addition to experiments, predicts the complete time evolution of both core CdS and core−shell CdS−ZnS nanoparticle diameter. Formation of shell is characterized by a sudden increase in nanoparticle diameter in the simulation curves at time $t = 200$ s (Figure 3), corresponding to the addition of microemulsion C and the formation of ZnS at that instant of time. It is thus seen that ZnS formation and deposition as shell on the core CdS occurs quickly, leading to a very short transition period in the evolution of shell thickness and thereby achieving a constant core−shell diameter. Such a feature in simulation results points to a fast dynamics in shell formation and growth, facilitated by coalescence-exchange of drops. Based on these comparisons, we can conclude that our mechanism and resultant simulation scheme is able to capture the core−shell nanoparticle formation process quantitatively in most cases.

For each experimental run, we also measured a series of UV−vis spectra, which were recorded as a function of time. To the best of our knowledge, there is no method available to calculate evolving core−shell nanoparticle diameter from UV−vis spectra as it is not clear how the two materials combine to result in the spectral peak and shoulder. Therefore, to estimate the temporal evolution of the outer diameter of CdS−ZnS core−shell nanoparticles, we approximated the CdS−ZnS core−shell particle to consist of a pure CdS particle only. This seems a reasonable approximation, as the shell thickness of 0.35 to 0.8 nm is only about 15% of the outer radius of the core−shell nanoparticles, so that most of the nanoparticle is only CdS. A reasonably close match between this approximate experimental estimate of the temporal evolution of outer diameter of CdS−ZnS core−shell nanoparticle (open circular and triangular symbols) with prediction from simulation (solid curve) is seen for the case in which $R = 15$. For other values of *R*, there is a large deviation between simulation and approximate experimental estimate of core−shell diameter. Thus, the above approximation for calculating temporal evolution of core−shell nanoparticle diameter seems to be good when the nanoparticle itself is of large diameter, but is inappropriate for smaller nanoparticles obtained in smaller drops ($R = 2$ to 10).

Our UV−vis experiments for both core and core−shell nanoparticles have been repeated at least thrice for each value of *R* and are quite reproducible within a calculated diameter of about ± 0.1 nm (Figure 3). Each UV−vis scanning in our instrument takes about 120 s. Therefore, the instants of time at which the experimental data are reported in Figure 3 are the mean of the above scan-time period. As a result, we do not have more experimental data points at shorter times for following the evolution of core nanoparticle diameter.

Overall, both CdS and CdS−ZnS nanoparticle diameter increases with the drop size of w/o microemulsions based on UV−vis measurements and mass balance estimate. This is quantitatively predicted from our simulation and justifies the proposed mechanism in all cases, except when the nature of water is known to be very different from bulk water at small *R* (i.e., small microemulsion drop size). In addition, we propose a new approximate method of estimating the temporal evolution of outer diameter of CdS−ZnS core−shell nanoparticle, utilizing the available UV−vis spectra measured by us. This again works well for large nanoparticles obtained in larger drops.

4. Conclusions

CdS−ZnS core−shell nanoparticles of a controlled diameter in the 3−10 nm range have been synthesized by mixing reactive w/o microemulsion solutions. Size control is achieved by changing microemulsion drop size on altering water to surfactant molar ratio (*R*) from 2 to 15. As a result, the particle diameter also increases with *R*. This reflects the control offered by the self-assembled template structure and size in core−shell nanoparticle synthesis. Based on our experimental observation that the shell component (ZnS) neither nucleates itself nor undergoes coagulation with other core−shell nanoparticles, we have proposed a mechanism of core−shell nanoparticle formation. We further developed a MC simulation scheme of this mechanism. Simulation takes into account the two sequential phases followed in experimental synthesis: core nanoparticle formation and shell growth. The first phase is the formation of CdS nanoparticles by reaction and nucleation, followed by growth through both coalescence-exchange and particle coagulation. The second phase occurs by reaction leading to ZnS formation and further coalescence-exchange leading to deposition and growth of a ZnS shell around CdS nanoparticles. Simulation results explain our experimental data on both core CdS particle diameter and final ZnS shell thickness for most of the cases ($R = 6$, 10, and 15), except for $R = 2$. The latter mismatch is ascribed to the known effect of different nature of water at low values of *R*.

Our framework is applicable to any other self-assembled structure, which is distinguished based on their confinement length scale and collision dynamics. These features are integrated in our mechanism and are accounted for in simulation. Thus, the present simulation and its extension can give insight to the understanding of the formation of core−shell or other heterostructures in different kinds of self-assembled aggregates. This allows control of particle diameter and properties by manipulating template size, shape, and reactant concentration.

Acknowledgment. We gratefully acknowledge Professor Sanjeev Garg, Chemical Engineering Department, IIT Kanpur, for letting us use Elico SL159 UV−vis spectrophotometer.

References and Notes

(1) Nirmal, M.; Brus, L. *Acc. Chem. Res.* **1999**, *32*, 407.
(2) Alivisatos, A. P. *J. Phys. Chem.* **1996**, *100*, 13226.
(3) Qu, L.; Peng, X. *J. Am. Chem. Soc.* **2002**, *124*, 2049.
(4) Talapin, D. V.; Rogach, A. L.; Konowski, A.; Haase, M.; Weller, H. *Nano Lett.* **2001**, *1*, 207.
(5) Mekis, I.; Talapin, D. V.; Konowski, A.; Haase, M.; Weller, H. *J. Phys. Chem. B* **2003**, *107*, 7454.
(6) Peng, X.; Schlamp, M. C.; Kadavanich, A. V.; Alivisatos, A. P. *J. Am. Chem. Soc.* **1997**, *119*, 7019.
(7) Dabbousi, B. O.; Rodriguez-Viejo, J.; Mikulec, F. V.; Heine, J. R.; Mattoussi, H.; Ober, R.; Jensen, K. F.; Bawendi, M. G. *J. Phys. Chem. B* **1997**, *101*, 9463.
(8) Youn, H. C.; Baral, S.; Fendler, J. H. *J. Phys. Chem.* **1998**, *92*, 6320.
(9) Hirai, T.; Shijori, S.; Komasawa, I. *J. Chem. Eng. Jpn.* **1994**, *27*, 590.
(10) Loukanov, A. R.; Dushkin, C. D.; Papazova, K. I.; Kirov, A. V.; Abrashev, M. V.; Adachi, E. *Colloids Surf., A.* **2004**, *245*, 9.
(11) Qi, L.; Ma, J.; Cheng, H.; Zhao, Z. *Colloids Surf., A.* **1996**, *111*, 195.
(12) Zhou, H. S.; Honma, I.; Komiyama, H.; Haus, J. W. *J. Phys. Chem.* **1993**, *97*, 895.
(13) Hasselbarth, A.; Eychmuller, A.; Eichberger, R.; Giersig, M.; Mews, A.; Weller, H. *J. Phys. Chem.* **1993**, *97*, 5333.
(14) Hota, G.; Jain, S.; Khilar, K. C. *Colloids Surf., A.* **2004**, *232*, 119.
(15) Han, M. Y.; Huang, W.; Chew, C. H.; Gan, L. M.; Zhang, X. J.; Ji, W. *J. Phys. Chem. B* **1998**, *102*, 1884.
(16) Murray, C. B.; Norris, D. J.; Bawendi, M. G. *J. Am. Chem. Soc.* **1993**, *115*, 8706.
(17) Pileni, M. P. *Adv. Colloid Interface Sci.* **1993**, *46*, 139.
(18) Peng, X. G.; Wickham, J.; Alivisatos, A. P. *J. Am. Chem. Soc.* **1998**, *120*, 5343.
(19) Bagwe, R. P.; Khilar, K. C. *Langmuir* **2000**, *16*, 905.
(20) Hirai, T.; Sato, H.; Komasawa, I. *Ind. Eng. Chem. Res.* **1994**, *33*, 3262.
(21) Roman, J.-P.; Hoornaert, P.; Faure, D.; Biver, C.; Jacquet, F.; Martin, J.-M. *J. Colloid Interface Sci.* **1991**, *144*, 324.
(22) Marciano, V.; Minore, A.; Turco Liveri, V. *Colloid Polym. Sci.* **2000**, *278*, 250.
(23) Debuigne, F.; Jeunieau, L.; Wiame, M.; Nagy, J. B. *Langmuir* **2000**, *16*, 7605.
(24) Pileni, M. P.; Zemb, T.; Petit, C. *Chem. Phys. Lett.* **1985**, *118*, 414.
(25) Zana, R.; Lang, J. Dynamics of microemulsions. In *Microemulsions: Structure and Dynamics*; Friberg, S. E., Bothorel, P., Eds.; CRC Press: Boca Raton, Florida, 1987; pp 153−172.
(26) Wang, Y.; Suna, A.; Mehler, W.; Kasowski, R. *J. Chem. Phys.* **1987**, *87*, 7315.
(27) Brus, L. E. *J. Chem. Phys.* **1984**, *80*, 4403.
(28) Vossmeyer, T.; Katsikas, L.; Giersig, M.; Popovic, I. G.; Diesner, K.; Chemseddine, A.; Eychmuller, A.; Weller, H. *J. Phys. Chem.* **1994**, *98*, 7665.
(29) Israelechvili, J. *Intermolecular & Surface Forces*; Academic Press: San Diego, CA, 2003.
(30) Jain, R.; Shukla, D.; Mehra, A. *Langmuir* **2005**, *21*, 11528.
(31) Burgess, J. *Metal Ions in Solutions*; Ellis Horwood: Chichester, England, 1978.
(32) Jain, R.; Shukla, D.; Mehra, A. *Ind. Eng. Chem. Res.* **2006**, *45*, 2249.
(33) Bandyopadhyaya, R.; Kumar, R.; Gandhi, K. S. *Langmuir* **2000**, *16*, 7139.
(34) Ethayaraja, M.; Dutta, K.; Bandyopadhyaya, R. *J. Phys. Chem. B* **2006**, *110*, 16471.
(35) Ethayaraja, M.; Bandyopadhyaya, R. *J. Am. Chem. Soc.* **2006**, *128*, 17102.
(36) Infelta, P. P.; Graglia, R.; Minero, C.; Pelizzetti, E. *Colloids Surf.* **1987**, *28*, 289.
(37) Shah, B. D.; Ramkrishna, D.; Borwanker, J. D. *AIChE J.* **1977**, *23*, 897.
(38) Smoluchowski, M. V. *Phys. Z.* **1916**, *17*, 557.
(39) Bandyopadhyaya, R.; Kumar, R.; Gandhi, K. S. *Langmuir* **2001**, *17*, 1015.
(40) Kandori, K.; Kon-No, J.; Kitahara, A. *J. Colloid Interface Sci.* **1988**, *122*, 78.
(41) Hirai, T.; Sato, H.; Komasawa, I. *Ind. Eng. Chem. Res.* **1993**, *32*, 3014.